Flattening of the electric permittivity curve ε(*T*) of $NaNbO_3$:*y*Mn single crystals caused by stress application

2001 J. Phys.: Condens. Matter 13 9561

(http://iopscience.iop.org/0953-8984/13/42/315)

INSTITUTE OF PHYSICS PUBLISHING JOURNAL OF PHYSICS: CONDENSED MATTER

J. Phys.: Condens. Matter **13** (2001) 9561–9573 PII: S0953-8984(01)25456-3

Flattening of the electric permittivity curve $\varepsilon(T)$ of $NaNbO_3$:*y*Mn single crystals caused by stress application

A Molak

Institute of Physics, University of Silesia, ul. Uniwersytecka 4, PL-40-007 Katowice, Poland

E-mail: molak@us.edu.pl

Received 4 June 2001
Published 5 October 2001
Online at stacks.iop.org/JPhysCM/13/9561

Abstract

A DTA test, performed within the 300–700 K range, showed that the series of $NaNbO_3$:*y*Mn single crystals exhibit first-order phase transition known from pure sodium niobate. The introduced Mn dopant lowers the temperature of this phase transition at a rate $\Delta T_{P-R}/\Delta\%(Mn) \approx -15$ K wt%$^{-1}$. The electric permittivity measured at ambient pressure showed a clear Curie–Weiss maximum at this antiferroelectric phase transition. The applied axial compression caused gradual suppression of this anomaly towards step-like characteristics. Flat $\varepsilon(T, X, y)$ curves appeared when the axial pressure X exceeded a few hundreds bars. The stress field was calculated around the Mn ions built into the host. It was pointed out that due to this the stress field and external compression are lower than misfit stress estimated for the P–R structural phase transition and any new phase was not induced with dopant manganese ions at the obtained real concentration y level. The recorded $\varepsilon(T, X, y)$ characteristics were fitted with a generalized Curie–Weiss formula. It was shown that the molecular field approximation remains valid. Both linear and nonlinear elastic effects were necessary to describe the experimental $\varepsilon(T, X, y)$ characteristics.

1. Introduction

Sodium niobate ($NaNbO_3$) is a focus of attention as a compound for solid solutions that shows a combination of electrical and mechanical properties required for application materials. Sodium niobate exhibits a sequence of phase transitions lowering the symmetry of the perovskite lattice from cubic through orthorhombic. The phases show paraelectric or antiferroelectric order and the structural phase transitions are connected to anomalies in electric permittivity. The Curie–Weiss-type anomaly ascribed to soft-mode behaviour [1] appears at a first-order transition that occurs between antiferroelectric phases (called P and R) with hysteresis between

644 and 617 K. Additionally, ferroelasticity appears in the low-symmetry phase. Although pure sodium niobate does not show ferroelectric order [2], it can be induced with strong electric field [3]. However, ferroelectric phases could be found in a variety of its solid solutions.

A potential use in high-temperature piezoelectric devices and even acoustic transducers operating in the microwave range is possible when ferroelectric properties are induced in $NaNbO_3$-based solid solutions. The required ferroelectric solid solution can be obtained with isovalent niobates, e.g. $LiNbO_3$, $KNbO_3$, [4, 5] and $AgNbO_3$ [6]. The other method is based on ceramic systems containing heterovalent substitution: $NaNbO_3$–$A^{II}Nb_2O_6$, where A^{II} means a bivalent ion, and among others, systems where Ba, Ca, Mn, Pb, Zn, replace the Na ion. The values of several coefficients, varying with the A^{II}-ion concentrations, concerning the ferroelectric phases that appeared in $NaNbO_3$-based ceramic solid solutions, were reported [4, 5].

On the other hand, single crystals of $NaNbO_3$ doped with manganese did not show ferroelectric properties although another new phase was induced with the Mn dopant [7]. It should be mentioned that, in the case of these sodium niobate single crystals, Mn ions are built into the Nb sub-lattice [8].

Another point of interest concerning application use relates to the high value dielectric constant with weak temperature dependence. Such flat $\varepsilon(T)$ curves (values of the order of thousands) have been obtained in relaxor perovskite materials and related tungsten-bronze-type niobates [9, 10]. Similar properties are hard to obtain within the simple perovskite $NaNbO_3$ but quite a weak temperature dependence of the dielectric constant, $\varepsilon(T)$ value about 50, was observed on an oriented a-domain sample below room temperature: 300 K down to 20 K [2].

The conditions required to produce flat dielectric constant characteristics of $NaNbO_3$ single crystals that were doped with Mn ions or when the crystals were under axial compression are reported in this paper.

2. Experimental

2.1. Sample preparation

Single crystals of sodium niobate were grown by the flux method from a melted salt solution. A mixture of Na_2CO_3 (Reachim, purity $\geqslant$99.8%), Nb_2O_5 (Aldrich, purity $\geqslant$99.9%) and Ba_2O_3 (Aldrich, purity 99%) solvent was used [11]. Manganese oxide (Puratronic JVC, purity 99.999%) was added to the obtained solution and the $NaNbO_3$ crystals remelted. The mixtures were prepared to obtain a nominal content of Mn equal to 0, 1, 2, 5 and 10 wt%. The real content of the doped Mn ions in sodium niobate crystals happend to be one order lower [8].

2.2. DTA test

The DTA test was performed using Unipan DSC 605 equipment. The as-grown and crushed single crystals with diameters $\sim$0.1–1 mm were enclosed in gaskets. The DTA signals were recorded in the 300–700 K range while temperature change rates were $\pm$5 or $\pm$8 K min^{-1}.

2.3. Dielectric measurement

The electric permittivity was measured with a Meratronic RLC E318 capacitance meter. The measuring frequency was equal to 1 kHz. The electrodes were painted with Ag paste and fired. The temperature was varied within the range 300–700 K at a constant rate of change

1 K min^{-1} with the use of a Unipan Temperature Controller type 680. Axial compression was applied to the bar samples with the use of a lever and a weight within the range $X =$ 1–1000 bar with accuracy ∼10 bar. The sample crashed when higher pressure was applied. Capacitance and loss factor were recorded under constant pressure in subsequent cycles of heating and cooling. The bar samples were chosen from as-grown single crystals whose edges were parallel to the axes of paraelectric cubic phase existing above 910 K. The data collection and processing were made with the use of a PC unit.

3. Results and discussion

3.1. DTA

The crystals of sodium niobate doped with manganese were grown in the form of rectangular bars or plates and their edge dimensions were of the order of millimetres. At room temperature, they showed domain structure, which appeared after a sequence of structural phase transitions (between phases called C, T_2, T_1, S and R) to the antiferroelectric phase (called P). At room temperature the samples were in a multi-domain state of the antiferroelectric and ferroelastic phase, which was reported as orthorhombic in orientation [12] or monoclinic [13]. The DTA test confirmed the non-continuous, first-order phase transition between phases P and R. A small bump visible near 680 K could be connected to formation of phase I induced by dopant manganese ions. It was reported for ceramic $NaNbO_3$:yMn that the phase I coexists with phase P when the dopant concentration y is high enough [7, 14] (figure 1).

The dopant manganese ions caused a decrease in temperature $T_{P–R}$ of this phase transition. The real content of the Mn ions in the sodium niobate crystals happened to be one order lower than the nominal. As stated earlier, lower real concentrations of Mn dopant were experimented on by different methods [8, 15, 16] for a defined nominal content. This effect is consistent with inhomogeneous distribution of this dopant within the $NaNbO_3$:Mn samples shown by microanalysis [15]. After that, different Mn concentrations were found even for various samples taken from the same grown process [8] (compare data given in table 1 and figure 2). The low real concentration of the manganese dopant was related to the solubility limit in the sodium niobate crystal as ≈1 wt% [8]. It should be mentioned that ≈1 wt% of Mn corresponds to 3 mol% of Mn in sodium niobate. This value is comparable with a solubility limit $y \approx 5\%$ found in ceramic solid solution $(1 - y)\,NaNbO_3 - y Mn_{0.5}NbO_3$ [5]. Thus the real rate of $T_{P–R}$ lowering was estimated approximately as $\Delta T_{P–R}/\Delta\%(\mathrm{Mn}) \approx -15$ K wt%$^{-1}$. Due to nonuniform Mn dopant distribution within the $NaNbO_3$:Mn samples a higher (-40 K wt%$^{-1}$) or lower (-11 K wt%$^{-1}$) boundary rate might also be accessible.

3.2. Electric permittivity ε(T, X, y)

Electric permittivity of sodium niobate crystals, pure (0%) or doped nominally with 1, 2 or 5% of Mn, measured at ambient pressure, showed a clear Curie–Weiss-type maximum at the phase transition. The applied axial compression X caused gradual suppression of this anomaly towards step-like characteristics (see figures 3(a) and (b)). Flat $\varepsilon(T, X, y)$ curves appeared when the pressure exceeded a few hundred bars. This effect was reversible—the Curie–Weiss anomaly recovered after several heating–cooling cycles performed at ambient pressure. In the case of samples doped with nominally 10% of Mn, electric permittivity exhibited a mild maximum at ambient pressure and the $\varepsilon(T, X, y)$ curves became flat on account of weak pressure starting from a few bar of compression applied (see figure 3(c)). Additionally,

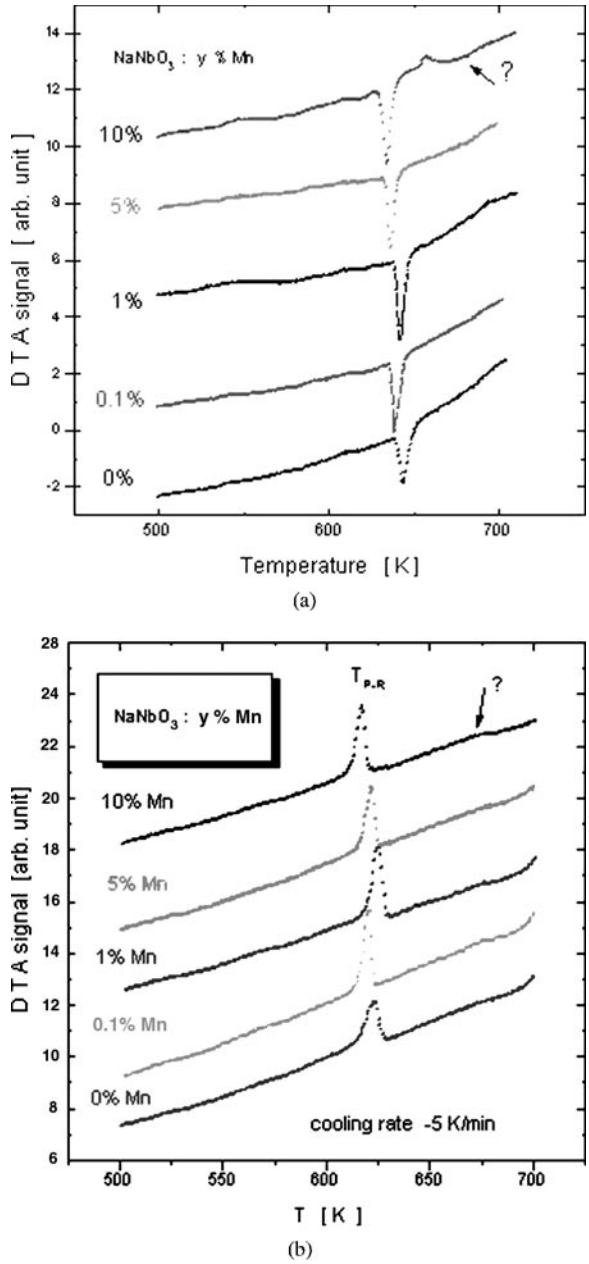

Figure 1. DTA signal recorded on (a) heating and (b) cooling for crystal samples of $NaNbO_3$:yMn. Nominal content $y = 0$, 1, 5 and 10 mol%.

while $X > 1$ bar, the recorded $\varepsilon(T, X, y)$ characteristic exhibited a sequence of jumps within the range of the concerned phase transition. This step-like evolution manifested an athermal martensitic behaviour induced with stresses as discussed earlier [7]. The weak dependence of dielectric constant on temperature outside the phase transition range was significantly above

Table 1. Nominal and real content of Mn ions in single crystals of $NaNbO_3$:yMn grown with nominal Mn concentration $y = 0$, 1, 2, 5 and 10 mol% which exhibited lower real Mn content. The Mn dopant caused a shift in parameters (determined from DTA) of transition between phases P and R: temperature of the transition, $T_{P–R}$; heat, $Q_{P–R}$ and entropy, $\Delta S_{P–R}$ of the transition. Comment: (A) $NaNbO_3$, pure, no MnO_2 added, growing process by Dec [11], no traces of Mn^{2+} ions detected by EPR. (B) $NaNbO_3$:yMn, grown by Dec [11] with nominally $y = 1\%$ Mn, real Mn content approximated. (C) $NaNbO_3$:yMn, grown by Jelonek [15] with nominally $y = 2$ wt% Mn], real Mn content: 0.11–0.31 wt% checked with microanalyser, Mn precipitations were found [15]. (D) $NaNbO_3$:yMn, grown by Dec [11] with nominally $y = 5\%$ Mn, (#) real content 0.4–0.6 wt% Mn estimated with XPS [8], (∗) real content 0.04 wt% with atomic emission spectrometry [16]. (E) $NaNbO_3$:yMn, grown by Dec [11] with nominally $y = 10\%$ Mn, (#) real content 0.6–1.0 wt% Mn estimated by XPS [8], (∗) real content 0.3 wt% Mn with atomic emission spectrometry [16].

	Nominal content	Real (wt% Mn)	$T_{P–R}$ (K)	$Q_{P–R}$ (DTA) (J mol^{-1})	$\Delta S_{P–R}$ (J mol^{-1} K^{-1})
A	0%	0	644	210	0.32
B	1%	≈0.05	642	230	0.35
C	2%	0.1–0.3	639	250	0.39
D	5%	0.4–0.6$^{\#}$ 0.04*	636	270	0.42
E	10%	0.6–1.0$^{\#}$ 0.3*	632	280	0.44

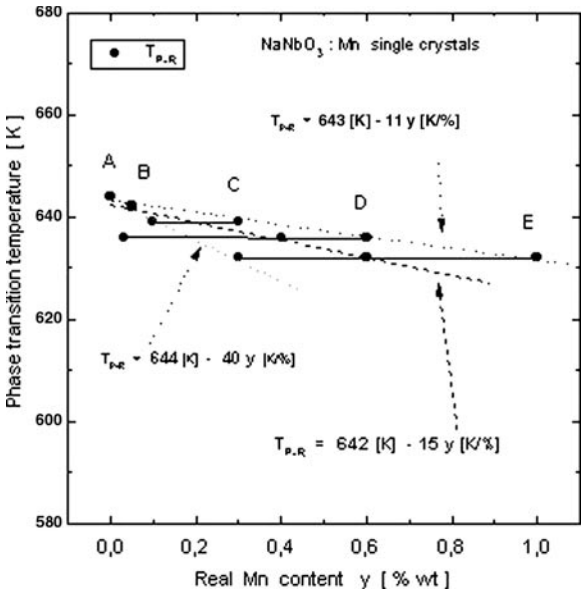

Figure 2. Diagram of P–R phase transition temperature versus real Mn content in $NaNbO_3$:yMn single crystals. Various concentrations obtained with different methods lead to higher or lower values of the rate $\Delta T_{P–R}/\Delta\%$(Mn).

$T_{P–R}$, within the antiferroelectric phase called R, when the samples were compressed or doped with Mn highly enough.

The common possible mechanism that leads to the obtained flatness of $\varepsilon(T, X, y)$ curves can be ascribed to stress–strain effects. Those occurring here have two main sources: one is caused by external pressure and the other is due to the stress field around the dopant ions.

It is seen in figure 3 that when the axial pressure exceeds about 100 bars and reaches 1000 bars then the recorded $\varepsilon(T, X, y)$ curves converge to those appearing for non-compressed $NaNbO_3$:Mn crystals doped highly enough (10% nominally, that is the real concentration $\approx$1 wt% Mn). The external stress was also able to modify the kinetics of the inter-phase boundary that was reflected in step-like characteristics of $\varepsilon(T, X, y)$ in the vicinity of the phase transition. One can point out that even such quite moderate external stress may act efficiently during the phase transition when the crystal lattice becomes soft (see step-like jump in figure 3) [7, 17, 18].

At a noncontinuous phase transition in sodium niobate, the lattice constants' differences in the P and R phases produce a mismatch stress. The resulting elastic strains can be accommodated by the formation of an array of edge dislocations at the interface boundary. Additionally, point defects like oxygen vacancies or Mn dopant ions act as stress concentrators. Mismatch stress ought to be proportional to Young's modulus, C times lattice constants misfit at the boundary between phases P and R.

The values of strain tensor components, connected to the considered P–R phase transition, are $e_a = \Delta a/a_0 = -0.001\,1722$, $e_b = \Delta b/b_0 = 0.001\,4051$, $e_c = 0$, $t = \tan((\delta - 90^\circ)/2) = 0.0017$ [19]. Such strains cause stresses, which can be estimated with the use of Hooke's law. This equation is written here not as a tensor equation but in the form of a relation between effective quantities, due to multi-domain samples being used for the experiment,

$$\sigma = Cu. \tag{1}$$

The Young's modulus for pure sodium niobate is not known exactly but such a parameter was determined [20] for a $(Ba_{0.1}Na_{0.9})(Ti_{0.1}Nb_{0.9})O_3$ solid solution: $1/s_{11} = 1.135 \times 10^{11}$ N m^{-2}. Taking $C \approx (1/s_{11})$ as the effective value and the approximate value of the strain component as $u_e \approx 10^{-3}$ one obtains misfit stress, overstepping 10^8 Pa = 1000 bar level, that appears near the phase front during P–R phase transition.

Hooke's law also allows estimation of stresses produced by dopant ions in their surroundings. The strain u_d at distance r from a dopant ion can be evaluated as

$$u_d = [(R_d - R_m)/R_m](R_m/r)^3 \tag{2}$$

where R_d denotes the radius of the dopant ion and R_m the radius of the replaced host ion [21].

Two cases should be considered: first when Mn ions replace Nb ions [8] and second when Mn is built into the Na sub-lattice [22, 23]. The oxygen perovskite crystals exhibit not purely ionic but mixed covalent–ionic character and thus, the effects of valence and coordination number should be considered in order to calculate strains and stresses produced around dopant ions. The niobium ions are surrounded by six oxygen ions forming a octahedron. The sodium position in $NaNbO_3$ with low-symmetry phase (Pbcm) at room temperature is more complicated. Due to distortions, the surrounding 12 ions that exist in the cubic perovskite phase are actually changed. Two non-equivalent positions are distinguished, characterized by lowered number of nearest neighbours, namely Na(1) with 8nn and Na(2) with 4nn [12].

Instead of traditional ionic radii, the crystal radii listed for different coordination numbers reported by Shannon [24] were taken for calculation. The results are presented in table 2. Calculated strains, at a distance 1 nm, are of the order of 10^{-4}. Taking again as the effective value $C \approx (1/s_{11}) = 1.135 \times 10^{11}$ N m^{-2}, the stresses produced within the samples were estimated. Tensile $\sigma_{Mn(Nb)} = +130 \times 10^5$ Pa stress should exist around the Mn^{2+} dopant replacing the Nb ions. The Mn^{3+}_{Nb} ions would create vanishing small stress. All three other substitutions could generate compressive stresses, from -80×10^5 Pa to -480×10^5 Pa.

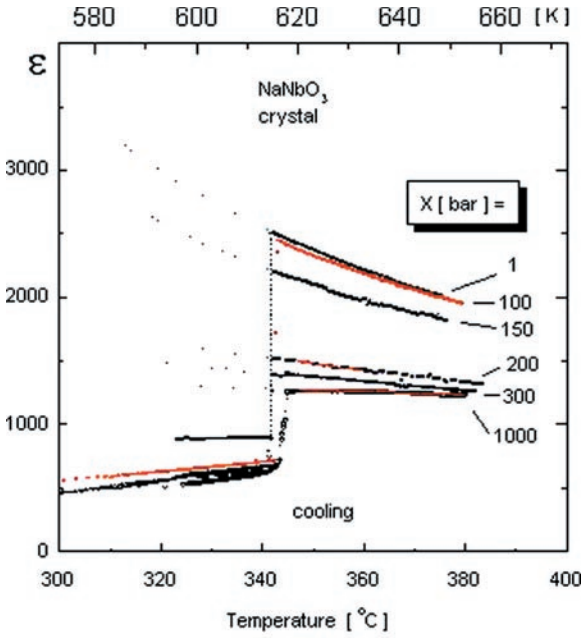

(a)

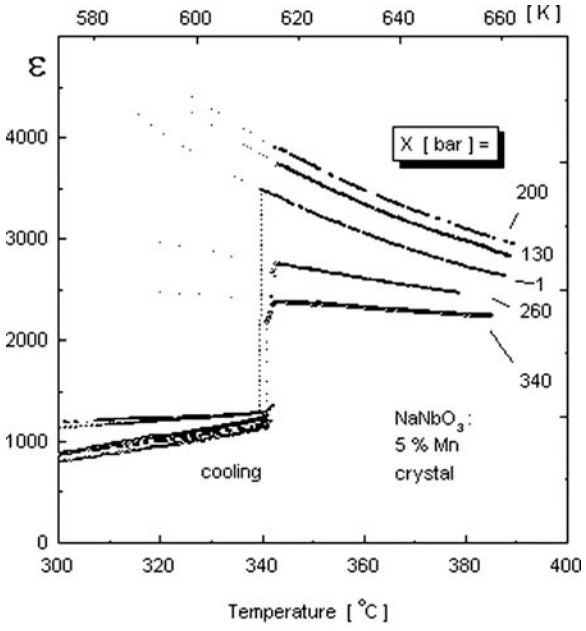

(b)

Figure 3. Electric permittivity versus temperature of sodium niobate single crystals recorded under various axial pressure X (bar): (a) pure $NabO_3$, (b) $NaNbO_3$:yMn, nominally $y = 5\%$, (c) $NaNbO_3$:yMn, nominally $y = 10\%$. Extrapolated lines (- - -) were obtained with the modified Curie–Weiss formula (equation (11)) from $\varepsilon\ (T, X, y)$ data recorded within the high-temperature R phase.

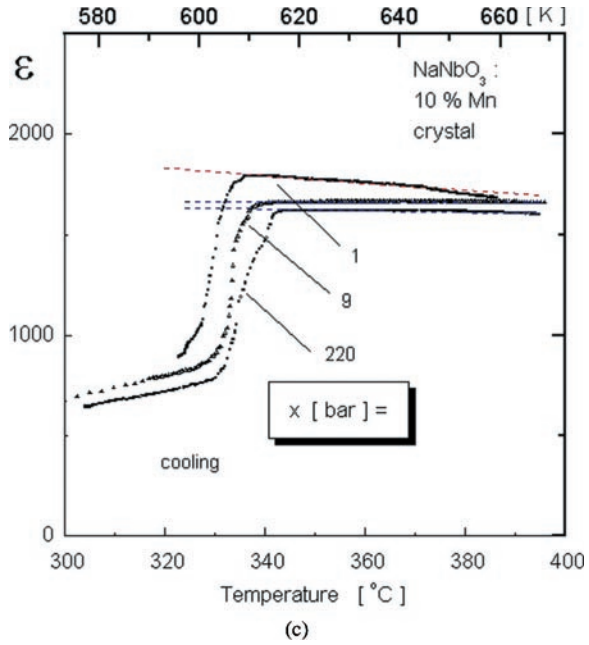

Figure 3. (*Continued*)

The calculation supported on the 'traditional' effective ionic radii gave similar values of stress and strain but several per cent lower. Only Mn^{2+} built into the Nb^{5+} sub-lattice creates tensile stress, $+90 \times 10^5$ Pa, and the other substitution gave compressive stresses within a range from -30×10^5 Pa to -370×10^5 Pa.

The case of tensile stress, when Mn^{2+} ions replace Nb^{5+} ions, corresponds to an increase in the elementary cell caused by the Mn dopant in $NaNbO_3$ single crystals observed with x-ray

Table 2. Strain, u_d, and stress, σ, appearing when manganese ions replace Nb or Na ions. Calculated with formulae $u_d = [(R_d - R_m)/R_m](R_m/r)^3$ [21] and $\sigma = C\,u_d$, $C = 1.135 \times 10^{11}$ N m^{-2} [20]. Evaluation carried out for various numbers of nearest neighbours (nn) at distance $r =$ 1 nm. Crystal radii (CR) of dopant ions, R_d, and host ions, R_m, taken after Shannon [24] (values are in nm).

	Dopant ion (number of nn)			Host ion (number of nn)	Dopant ion (number of nn)		Host ion (number of nn)	
	Mn^{2+} (6nn)	Mn^{3+} (6nn)	Mn^{4+} (6nn)	Nb^{5+} (6nn)	Mn^{2+} (1) (8nn)	Mn^{2+} (2) (4nn)	Na^{1+} (1) (8nn)	Na^{1+} (2) (4nn)
R_d or R_m (nm)	0.097	0.0785	0.67	0.078	0.110	0.080	0.132	0.113
$R_d - R_m$ (nm)	0.019	0.0005	−0.011		−0.022	−0.033		
$(R_d - R_m)/R_m$	0.244	0.0006	−0.141		−0.167	−0.292		
u_d	1.16×10^{-4}	0.03×10^{-4}	-0.67×10^{-4}		-3.83×10^{-4}	-4.21×10^{-4}		
$\sigma = C\,u$ (Pa)	130×10^{-5}	3×10^{-5}	-80×10^{-5}		-435×10^{-5}	-480×10^{-5} Pa		

test [25]. The other probable situation is when Mn^{3+} ions replace Nb^{5+} ions at the cost of small elastic energy. The heterovalent Mn ions can be stabilized in both the cases with an oxygen vacancy [8]. If Mn^{2+} ions replaced Na^{+} ions then the change in elastic energy would be much higher. Anyway, the expected [22, 23] stabilization of Mn^{2+}_{Na} centres with niobium valence change ($Nb^{5+} \rightarrow Nb^{4+}$) was not detected [8].

The values of external axial pressure used in the experiment and the calculated internal stress produced by the Mn dopant in the obtained real concentration range were lower than the estimated misfit stress, occurring during the P–R phase transition. Therefore, they happened to be insufficient to induce any new stable phase in sodium niobate single crystals. However, one can deduce that such moderate stresses are sufficient to cause a shift in temperature in the P–R phase transition (DTA peak shift in figure 1, $T_{P–R}$ lowering in figure 2). Such stresses are also able to modify the kinetics of the interphase boundary that is reflected in the step-like curve $\varepsilon(T, X, y)$ characteristic in the vicinity of this phase transition [7, 17, 18].

The step-like jumps in $\varepsilon(T, X, y)$ curves, observed both for stressed samples (figures 3(a) and (b)) and for non-stressed but doped samples (figure 3(c)), can be compared. One can also deduce that the external and internal stresses appearing in the experiment (see figure 3 and table 2) carried out on sodium niobate crystals were efficient in producing flat electric permittivity characteristics within the high temperature phase. The flat curves occur when stresses are high enough ($\gtrsim$100 bar) or a certain dopant content (real concentration $\gtrsim$1 wt%) is overstepped. A potential application of sodium niobate-based materials, or even more generally niobates, in pre-stressed conditions demands a more detailed description of this effect [26].

3.3. Curie–Weiss-type dependence

Several reports can be found in the literature concerning pressure effects on phase transitions and electric properties of perovskite oxides. For instance, a new ferroelectric phase was induced in $SrTiO_3$ with an axial pressure $\gtrsim 10^8$ Pa, which corresponded to elastic strains about 3×10^{-4} [27]. In the case of $NaNbO_3$ an evolution of electric permittivity under hydrostatic pressure was reported and the flattening of this characteristic (apart from the phase transition temperature shift) was ascribed to a new phase induction [28].

When sodium niobate is treated as a system with an order parameter and antiferrodistortive mechanism, then three subsequent transitions between paraelectric phases (C, T_2, T_1, S) are generated [29]. The phase transitions to antiferroelectric phases, R, P (off-centre movement of Nb ions is involved [12]) are more complicated and more degrees of freedom should be included. Therefore, not only polarization but also a coupled stress subsystem should be considered.

To describe the recorded electric permittivity dependence both on temperature and stress, one can use the Landau approach to involve antiferroelectric (AFE) and elastic (EL) parts in free energy. The interplay between these instabilities is held to be responsible for the phase diagram of sodium niobate, as in other perovskite structures. The elastic part should include external effects appearing from axial compression and also local stresses due to strain caused by dopant ions. The axial symmetry of the crystal field around Mn^{2+} ions in sodium niobate has been found with an EPR experiment [22, 23]. Thus, the above estimated (equation (2)) local strain around Mn ions built into a sodium niobate host contains an axial component. Hence, the existence of a local distortion caused by such lattice defects leads to consideration of a non-linear, third-order, elastic term [30].

However, experimental values of several coefficients appearing in the free-energy expansion below are not known for sodium niobate. For instance, Young's modulus was

estimated for its solid solution [20]. Only one component of electrostrictive tensor, Q_{1111} (showing marked temperature dependence) has been determined within the P phase only [31]. For such reasons, necessary approximations were introduced to effectively conduct the fitting procedure of electric permittivity $\varepsilon(T, X, y)$ measured.

The modelling below is supported by theoretical calculus reported in the literature [30, 32, 33]. Electric permittivity dependence is derived from the Gibbs free energy for the given chemical composition

$$G(T, P, u) = U - TS - \sigma u - EP. \tag{3a}$$

From the equilibrium condition one gets electric and stress fields

$$\partial U/\partial u_{ij} = \sigma_{ij} \qquad \partial U/\partial P_i = E_i. \tag{3b}$$

Dielectric stiffness is defined as

$$\chi_{ij} = \partial E_i/\partial P_j \tag{3c}$$

and assuming a material with a high dielectric constant

$$\varepsilon_{ij}^{-1} \approx \chi_{ij}. \tag{3d}$$

The concerned sodium niobate remains in antiferroelectric phases P or R with low orthorhombic/monoclinic symmetry [12, 13]. The samples used in repeated cycles of heating and cooling during electric permittivity measurement were multi-domain. Therefore, because the measured quantities took effective values, tensor components are noted in simplified compact form below and subscripts are omitted.

The free energy consists of antiferroelectric (AFE), elastic (EL) and interaction (INT) parts

$$U = U_{\mathrm{AFE}} + U_{\mathrm{EL}} + U_{\mathrm{INT}} \tag{4a}$$

where

$$U_{\mathrm{AFE}} = U_{\mathrm{AFE0}}(T) + \tfrac{1}{2}a_1[T - T_0]P_{\mathrm{A}}^2 + \tfrac{1}{4}a_2P_{\mathrm{A}}^4 + \tfrac{1}{6}a_3P_{\mathrm{A}}^6 + \cdots \tag{4b}$$

$$U_{\mathrm{EL}} = U_{\mathrm{EL0}}(T) + \tfrac{1}{2}c_{\mathrm{L}}\,u^2 + \tfrac{1}{3}c_{\mathrm{NL}}\,u^3 + \cdots \tag{4c}$$

$$G_{\mathrm{INT}} = -\lambda u P_{\mathrm{A}}^2. \tag{4d}$$

When antiferroelectric phases are concerned, as in the case of sodium niobate, an average of sub-lattice polarization can be used in a free-energy expansion

$$P_{\mathrm{A}} = P_1 + P_2. \tag{5}$$

For the first order of P–R transition three terms in AFE expansion are taken with coefficients a_1, a_2 and a_3. Coefficients c_{L} denote the effective linear elastic stiffness ($\sim c_{ij}$) and u is the corresponding strain. Coefficient c_{NL} means non-linear elastic stiffness ($\sim c_{ijk}$) describing the effect of stress fields created by Mn dopant ions. The coupling of polarization and strain is described with electrostrictive coefficient λ.

From equations (3*b*) the obtained electric and elastic fields depend mutually on antiferroelectric polarization, strain and defect subsystem

$$\sigma = c_{\mathrm{L}}u + c_{\mathrm{NL}}u^2 + \lambda P_{\mathrm{A}}^2 \tag{6a}$$

$$E = a_1(T - T_0)P_{\mathrm{A}} + a_2P_{\mathrm{A}}^3 + a_3P_{\mathrm{A}}^5 - \lambda u P_{\mathrm{A}} - \lambda u^2 P_{\mathrm{A}}. \tag{6b}$$

A shift in phase transition temperature is obtained from the condition that polarization vanishes while the sample remains stressed

$$T_{\mathrm{A}}(\sigma) \cong T_{\mathrm{A}} - (\lambda/a_1)\left[s_{\mathrm{L}}\sigma - (s_{\mathrm{L}})^3 c_{\mathrm{NL}}\sigma\sigma\right]. \tag{7}$$

Inverting equation (6a) $\left((c_{ij})^{-1} \leftrightarrow s_{ij}\right)$ gives the related strain equation (as obtained by Freeman and Joshi [29]):

$$u_i = s_L\sigma_j - (s_L)(s_L)(s_L)c_{NL}\sigma_j\sigma_k - (s_L)\lambda(P_A)_j^2 - (s_L)(s_L)(s_L)c_{NL}\left(\lambda P_A^2\right)_j\left(\lambda P_A^2\right)_k + (s_L)(s_L)(s_L)c_{NL}\sigma_j\left(\lambda P_A^2\right)_k + (s_L)(s_L)(s_L)c_{NL}\left(\lambda P_A^2\right)_j\sigma_k. \quad (8)$$

After the relation (7) is substituted into equation (6c) the dielectric stiffness (3b) is obtained

$$\chi \approx \partial E/\partial P_A = a_1(T - T_0) + \lambda s_L\sigma - (s_L)(s_L)(s_L)c_{NL}\sigma\sigma - P_A^2\left(3a_2 - 3s_L \quad \lambda P_A^2 + \cdots\right) + \cdots. \quad (9)$$

Reciprocal electric permittivity can be written as

$$\varepsilon^{-1}(T,\sigma) \cong a(T - T_0)^1 + \left((P_A^*)^2 + \sigma^* + \sigma^{\#}\sigma^{\#}\right) \quad (10)$$

where P_A^*, σ^* and $\sigma^{\#}$ denote polarization and stress scaled with factors from the free-energy terms (compare equations (9) and (10)).

The formula obtained (10) was used to fit the experimental electric permittivity characteristics $\varepsilon(T, X, y)$ with a function

$$([1/P1][T - P2]^{(P3)} + P4)^{-1}. \quad (11)$$

The four parameters are interpreted as: $P1$—Curie–Weiss constant, C; $P2$—temperature of phase transition under stress, $T_0(\sigma)$; $P3$—Curie–Weiss exponent, γ; and $P4$—generalized effective stress, σ_{eff}, that includes effects of external stresses and defect-induced stress field appearing via non-linear elastic stiffness.

All the $\varepsilon(T, X, y)$ curves which had been measured in subsequent heating and cooling cycles at given external stress, were fitted satisfactorily with the formula (11) for the high-temperature phase R. The results are illustrated in figure 3 by dotted lines.

The values of fitting parameters depend on the external compression applied to the samples. The results for samples doped with 0, 2 and 5% Mn are as follows. $P1$ ($=C$) rises from 0.5×10^6 K up to 2×10^6 K. $P2$ ($=T_0(\sigma)$) changes with stress from ~470 K to ~620 K, $P3$ ($=\gamma$) takes the classic molecular field (Curie–Weiss formula) value 1 ± 0.2. $P4$ varies from 0 (for non-stressed or stressed below 100 bar samples) up to values $\approx 8 \times 10^{-3}$(while applied pressure was increased up to 1000 bar). For samples doped with 10% Mn: $P1$ rises from 1.1×10^6 up to 5×10^6 K, $P2$ changes between 10 and 540 K, $P3$ fluctuates around 0.95 ± 0.05 and $P4$ is always non-zero and equals $(5 \pm 0.5) \times 10^{-4}$. A detailed report concerning these fitting parameter dependences on the Mn dopant concentration and pressure is the subject of a prepared separate paper.

The calculation performed here distinguishes the pressure value ≈100 bar as a result of elastic effects introduced into the model. This calculated 'limit' or 'turning' value corresponds to the recorded experimental data of electric permittivity. It is seen in figures 3(a) and (b) that the experimental pressure of the order of 100 bar may also be considered as a turning value. Changes in the maximum value of electric permittivity for the lower axial pressure, in the range from ambient to 100–200 bar, can be connected to internal properties of the investigated samples, mainly to their domain structure. Sodium niobate samples contained point defects, which compose a variety of strains in their vicinity. From the point of view of energy, the strains generated by defects act as barriers that can be overcome by thermal activation and/or the applied stress. One can point out that the estimated stresses around Mn ions in the $NaNbO_3$:yMn lattice are of the same order as the obtained 'turning' value (100 bar, see table 2). On the other hand, sodium niobate exhibits complicated domain structure within both P and R

phases transforming one into the other [7, 8, 15, 18, 23]. The network of the domain walls may be affected by applied stress. For instance, such a phenomenon has been observed for axially compressed $SrTiO_3$ [34]. It seems that under low external pressure the domain walls are released leading to an increase in $\varepsilon(T, X, y)$ value. The measured effective electric permittivity depends on competitive phenomena resulting from domain structure and strains. The suppression of $\varepsilon(T, X, y)$ occurs when the stresses are sufficiently high and create additional strains: there are cases of nominal 10% doping (see figure 3(c)) or external compression overstepping the 'turning' value. These results remain in general agreement with the theoretical expectation about uniaxial pressure influence on discontinuous phase transitions [35].

4. Conclusions

In order to couple the strain to polarization both the effects from external axial compression and internal local stresses due to dopant ions have been considered. The linear and non-linear elastic terms are necessary and sufficient to describe the recorded $\varepsilon(T, X, y)$ characteristics within the proposed model. The modified Curie–Weiss dependence was successfully used for fitting the experimental data. The molecular field model remains valid because the Curie–Weiss exponent (parameter $P3 \equiv \gamma$) was equal to 1.

The calculated values of strain created by the manganese dopant, when compared to data from earlier literature, indicate that Mn ions are built into the Nb sub-lattice. The charge misfit is compensated most probably by oxygen vacancies. It should be pointed out that the stress field existing inside the sodium niobate samples has been modified by relatively low values of axial compression ($X < 1000$ bar) and low real content of Mn dopant ($y < 1\%$). The pressure and the defect concentration within these ranges were sufficient to induce marked changes in $\varepsilon(T, X, y)$ characteristics.

The dopant Mn ions form an active subsystem that influences the thermodynamic parameters of the antiferroelectric ferroelastic phase transition. Increasing the Mn content caused evolution of the electric permittivity towards flat step-like characteristics. The $\varepsilon(T, X, y)$ jump resulting from the P–R phase transition happened within a finite temperature interval. However, non-vanishing of the heat of transition indicates that the transition remains discontinuous. The local strains induced by the defects affect the stability of phases in $NaNbO_3$:yMn and shift the temperature $T_{P–R}$ of the transition between the P and R phases: the mean shift takes the value $\Delta T_{P–R}/\Delta\%(\mathrm{Mn}) \approx -15$ K wt%$^{-1}$. Moreover, it can be deduced that the stress field is locally inhomogeneous and causes a spatial variation of transition temperatures at the finite interval. Additionally, applied external axial compression strengthens this phenomenon.

Therefore, one should expect the common strain-based mechanism for the observed flattening of $\varepsilon(T, X, y)$ curves. The evolution of electric permittivity towards the flat characteristic can be controlled by a subsystem of active dopant ($y > 0.1\%$) and/or axial compression ($X > 100$ bar).

References

[1] Wang X B, Shen Z X, Hu Z P, Qin L, Tang S H and Kuok M H 1996 *J. Mol. Struct.* **385** 1
[2] Molak A, Onodera A and Yamashita H 1992 *Japan J. Appl. Phys.* **31** 3221
[3] Zhelnova O A, Fesenko O E and Smotrakov V G 1986 *Sov. Phys.–Solid State* **28** 144
[4] Reznitchenko L A, Dergunova N V, Geguzina G A, Razumovskaya O N, Shilkina L A and Ivanova L S 1997 *Inorg. Mater.* **33** 1277
[5] Reznitchenko L A, Geguzina G A and Dergunova N V 1998 *Inorg. Mater.* **34** 167
[6] Kania A and Kwapuliński J 1999 *J. Phys.: Condens. Matter* **11** 8933

[7] Molak A 1997 *J. Phys.: Condens. Matter* **9** 11 263
[8] Kubacki J, Molak A and Talik E 2001 *J. Alloys Compound.* **328** 156
[9] Haussonne J M, Desgardin G, Herve A and Boufrou B 1992 *J. Eur. Ceram. Soc.* **10** 437
[10] Boufrou B, Desgardin G, Haussonne J M and Lostec J 1993 *Silicates Ind.* **78** 149
[11] Dec J 1983 *Cryst. Res. Technol.* **18** 195
[12] Sakowski-Cowley A C, Łukaszewicz K and Megaw H D 1969 *Acta Crystallogr.* B **25** 851
[13] Darlington C N W and Knight K S 1999 *Acta. Crystallogr.* B **55** 24
[14] Molak A, Pawełczyk M and Kwapuliński J 1994 *J. Phys.: Condens. Matter* **6** 6833
[15] Molak A and Jelonek M 1985 *J. Phys. Chem. Solids* **46** 21
[16] Szot K 1999 private communication
[17] Tuszyński J A and Sept D 1994 *J. Phys.: Condens. Matter* **6** 3583
[18] Dec J 1993 *Phase Transit.* **45** 35
[19] Dec J and Kwapuliński J 1989 *Phase Transit.* **18** 1
[20] Khemakhem H, Simon A, Von Der Muhll R and Ravez J 2000 *J. Phys.: Condens. Matter* **12** 5951
[21] Lemanov V V 1999 *Ferroelectrics* **226** 133
[22] Bykov I P, Geifman I N, Deigen M D and Krulikovskii B K 1978 *Fiz. Tverd. Tela* **20** 622
[23] Molak A and Pichet J 1984 *Acta Phys. Pol.* A **66** 251
[24] Shannon R D 1976 *Acta Crystogr.* A **32** 751
[25] Molak A and Kubacki *J. Cryst. Res. Technol.* **36** 893
[26] Viehland D and Powers J 2001 *J. Appl. Phys.* **89** 820
[27] Fuji E and Sakudo E 1977 *Izv. Akad. Nauk* **41** 493
Sakudo T 1978 *Solid State Phys.* **13** 693
Currat R, Muller K A, Berlinger W and Denoyer F 1978 *Phys. Rev.* B **17** 2937
[28] Pisarski M 1980 *Acta Phys. Pol.* A **57** 693
[29] Vanderbilt D and Zhong W 1998 *Ferroelectrics* **206** 181
[30] Freeman A and Joshi S P 1999 *Ferroelectrics* **227** 1
[31] Miga S 1997 *PhD Thesis* University of Silesia, Katowice pp 65–8
[32] Blinc R and Zeks B 1974 *Soft Modes in Ferroelectrics and Antiferroelectrics* (Amsterdam: North-Holland)
[33] Okada K 1974 *J. Phys. Soc. Japan* **37** 1226
[34] Liu M, Finlayson T R and Smith T H 1997 *Phys. Rev.* B **55** 3480
[35] Fradkin M A 1994 *Phys. Rev.* B **50** 16 326